Volume 22
Number 18
13 May 2026
Pages 3279–3422

Soft Matter

rsc.li/soft-matter-journal

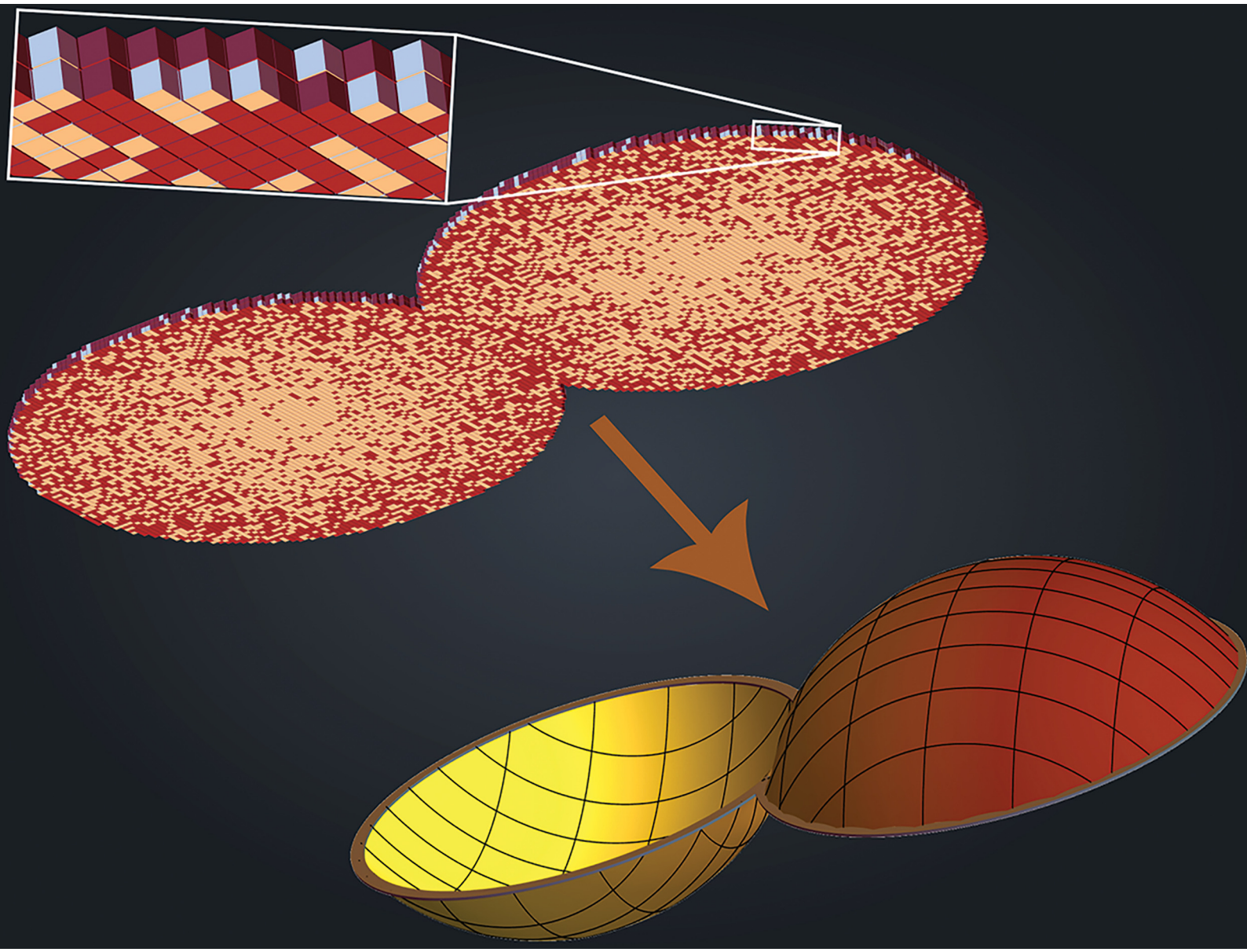

ISSN 1744-6848

ROYAL SOCIETY OF CHEMISTRY

PAPER
Ido Levin *et al.*
4D printing of fully programmable sheets of digital metamaterials

Soft Matter

PAPER

View Article Online
View Journal | View Issue

Cite this: *Soft Matter*, 2026, **22**, 3312

4D printing of fully programmable sheets of digital metamaterials

Ido Levin, *[abde] Ela Sachyani,[c] Rama Lieberman,[c] Noa Trink,[c] Eran Sharon[a] and Shlomo Magdassi[c]

Advances in 3D printing technology now enable the precise positioning of microscopic material voxels to form complex structures. Combined with emerging multi-material capabilities and printable responsive materials, this opens new possibilities for digital composite materials and 3D printing of shape-transforming structures, a process known as 4D printing. Building upon these advancements, we present a novel methodology for designing and fabricating digitized 4D-printed shape-transforming sheets. We 3D print responsive continuous sheets composed of two layers, each consisting of active and passive voxels meticulously positioned to form thin structures that transform on demand. Our approach addresses a long-standing challenge in the field: the independent and simultaneous programming of lateral geometry and intrinsic curvature. This unprecedented control over the resulting shape unlocks new opportunities in synthetic shape-morphing materials. We provide a general algorithmic approach that is material-agnostic and enables systematic design of shape transformations with potential capabilities for programmable mechanical properties and multi-actuation-mode systems and applications in soft robotics and deployable structures.

Received 30th July 2025,
Accepted 28th February 2026

DOI: 10.1039/d5sm00780a

rsc.li/soft-matter-journal

Introduction

The striking ability of many thin biological structures to induce intrinsic morphological changes relies on differential swelling – a non-uniform swelling of the structure.[1–3] The evolving shape is fully controlled by the local information encoded within the swelling magnitude and orientation at different locations. For thin sheets, differential swelling operates through two complementary orthogonal modes: the bilayer effect and Gaussian morphing.

Gaussian morphing involves inducing a lateral deformation gradient to program Gaussian curvature—a measure of how a surface curves in multiple directions simultaneously, like a saddle or a sphere. This enables, in principle, the realization of any 2D surface. However, there is no control over the bending direction (whether the surface curves upward or downward). The bilayer effect, by contrast, induces deformation gradients across the sheet thickness to program spontaneous curvature, which determines the bending direction and magnitude. This provides control over the direction of curvature but is limited to uniaxial curvature (bending in only one direction, such as a cylinder), resulting in surfaces with zero Gaussian curvature.

Therefore, to achieve complete control over the actuated shape, one must be able to impose both effects simultaneously. In other words, one must precisely program deformation gradients in 3D, in-plane, and through-thickness.

The potential of differential swelling for applications has inspired numerous multidisciplinary efforts to realize it using synthetic materials. Since small variations in swelling across the thin dimension of the sheet can induce large curvature magnitudes, most work has focused on programming spontaneous curvature[4–7] using the bilayer effect. More recently, researchers developed several techniques to induce Gaussian morphing precisely.[8–11] The actuated structures exhibit rich configurational phase space and can generate complex patterns through symmetry breaking in the programmed swelling fields. However, to date, the ability to fully prescribe a desired 3D shape in a solid sheet remains incomplete, as simultaneous and independent programming of both Gaussian and spontaneous curvatures has not yet been achieved.

The principal strategy for inducing differential swelling is through the use of responsive materials. These include hydrogels,[8,11–13] nematic elastomers,[9,10] and dielectric elastomers.[14] Selecting an appropriate material involves considering both the material properties and the method for programming differential swelling. Hydrogels are advantageous as they can be

[a] *Racah Institute of Physics, The Hebrew University, Jerusalem 91904, Israel*
[b] *Department of Chemistry, University of Washington, Seattle, WA 98195, USA*
[c] *Institute of Chemistry, The Hebrew University of Jerusalem, Jerusalem 9190401, Israel*
[d] *Department of Chemistry, University of British Columbia, Vancouver, BC V6T 1Z1, Canada. E-mail: ido.levin@ubc.ca*
[e] *Department of Mathematics, University of British Columbia, Vancouver, BC V6T 1Z1, Canada*

responsive to a variety of external stimuli, including temperature, pH, light, and humidity,[15,16] and can be actuated repeatedly. The response can be tailored to achieve relative volumetric shrinkage as high as 100-fold,[17] and hydrogel-based components are well-suited for integration into soft robots, implants, and drug delivery systems.[18–20] There has been growing interest in 3D-printed hydrogel structures, driven by advances in additive manufacturing.[21–26] Among the available 3D printing technologies, direct ink writing (DIW) and stereolithography (SLA), including digital light processing (DLP), are the most widely used for fabricating hydrogel structures.

Hydrogels offer several techniques for precise control of the swelling field. Lithography-based approaches enable very high spatial resolution.[11,27] Alternatively, shear alignment can be utilized to control the orientation of rigid fibers embedded within gel sheets, resulting in anisotropic swelling.[28] Some of these systems also provide limited through-thickness gradients *via* asymmetric polymerization[29] or by bonding two different layers.[30] However, complete three-dimensional control over the deformation field, which would enable arbitrary programming of target shapes, has not been achieved yet.

In this work, we present a novel 3D printing strategy for fabricating shape-morphing continuous hydrogel sheets with fully programmable 3D swelling gradients. This enables the actuation of both morphing modes simultaneously, yielding smart materials capable of achieving a broad range of programmable 3D shapes that are not accessible with only one morphing mode. Our approach is based on printing swelling gradients by digitizing the smooth swelling field and printing voxels with different swelling ratios (Fig. 1). This is analogous to how a conventional printers print grayscale gradients by printing black and white pixels. This pixelation strategy provides a general method to fabricate multi-material self-morphing structures, which applies to many printable responsive materials. Moreover, it can be readily extended to materials with anisotropic swelling response, such as nematic elastomers.

Specifically, we fabricate bi-material composite structures with an SLA 3D printer. Both materials are polyacrylic acid polymers crosslinked with polyethylene glycol diacrylate (PEGDA) but with different crosslinking densities, enabling the fabrication of two voxel types that swell by different ratios upon hydration. The relative spatial density of the printed voxels of each type determines the magnitude of the local swelling, just as the density of black pixels determines the grayscale value. At a coarse-grained scale, this digitization enables programming of continuous 3D swelling fields. By applying this digitization process independently to two layers, we create high-resolution digital 4D structures with a swelling ratio that can be programmed and controlled in 3D. This approach allows local determination of both the spontaneous and Gaussian curvatures, providing simultaneous and independent control over both shape-morphing modes.

The shaping of thin sheets *via* differential swelling can be formulated within the framework of non-Euclidean elasticity.[31] In this formalism, differential swelling is represented by geometric quantities: lateral swelling gradients are encoded in the reference metric, $\bar{a}$, and gradients across the thickness are encoded in the spontaneous curvature, $\bar{b}$. The programmed Gaussian curvature can be directly calculated from $\bar{a}$ (see SI). In many cases, $\bar{a}$ and $\bar{b}$ are incompatible, that is, no surface can simultaneously satisfy both $a = \bar{a}$, and $b = \bar{b}$, where, a, and b, are the *actual* metric and curvature tensors of the actuated shape, respectively. In such cases, the final shape is determined by a competition between bending and stretching energies. This

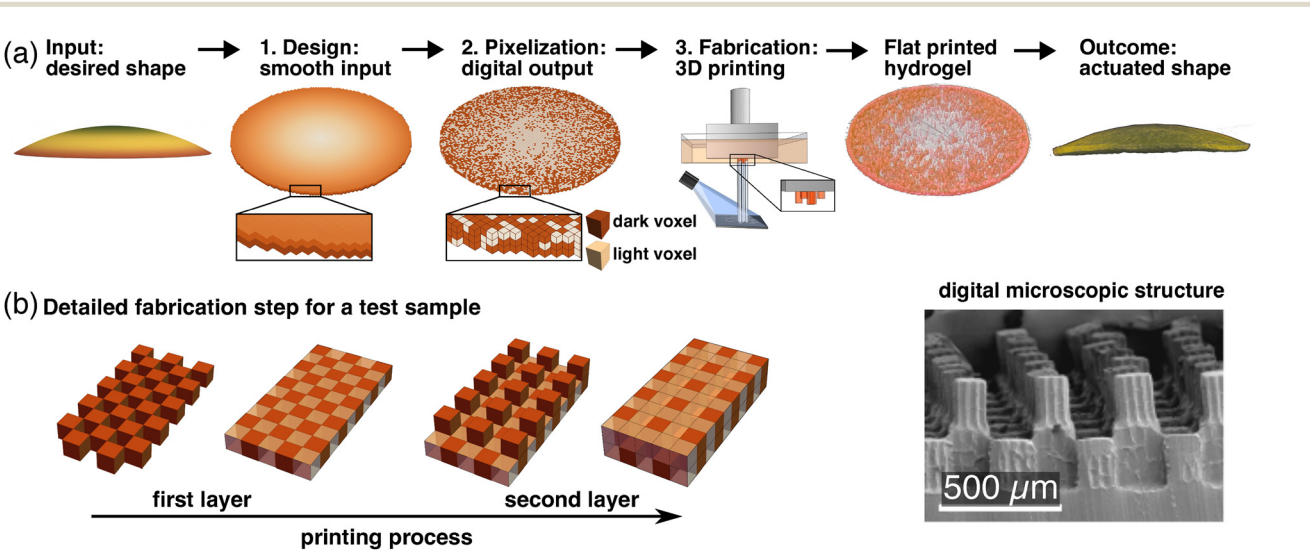

Fig. 1 Design, digitization, and fabrication. (a) Overview of our approach: (1) The geometry of the target shape is analyzed, resulting in its metric and curvature fields. The analysis yields a continuous conformal swelling density field for each layer. (2) The two continuous density fields are digitized into voxel patterns. (3) The digitized geometry is fabricated *via* multi-material 3D printing. The resulting flat sample is actuated in water, transforming into the desired 3D shape. (b) Detailed illustration of the fabrication process. A test voxelated bilayer structure consisting of two types of dark voxel stacks: 200 μm (a single voxel) and 400 μm (two stacked voxels). Multi-material printing process steps (left) and SEM image of the printed structure (right; only the dark voxels were printed for visualization).

competition gives rise to many of the rich phenomena observed in such systems: shape transitions,[4] symmetry breaking,[32,33] fractal structures,[34,35] and exotic mechanical properties.[36–38] To fully exploit these phenomena one must fully control the incompatibility, again calling for simultaneous programming of both shape-morphing modes.

Very thin sheets are nearly inextensible and hence, adopt configurations that obey the encoded lateral swelling gradients. In other words, very thin sheets realise the programmed Gaussian curvature. Therefore, an apparent strategy for designing a sheet that morphs into a desired shape is to program $\bar{a}$ that encodes the Gaussian curvature of that surface, a problem that can be solved analytically[11] or numerically.[39,40] However, specifying the metric alone is insufficient, as many different surfaces can share the same Gaussian curvature while having different shapes. Therefore, guiding the shape selection using $\bar{b}$, in addition to $\bar{a}$, is crucial.[13] For instance, programming a constant positive Gaussian curvature (corresponding to a spherical cap) will result in a bistable structure that can buckle upward or downward. The spontaneous curvature must also be prescribed to ensure buckling upward into a dome or downward into a cap. Indeed, the impressive control over $\bar{a}$ demonstrated in ref. 13 and 41 could guarantee the desired 3D shapes only in a limited range of cases. Moreover, when the sheet has finite thickness, bending effects emerge that cause deviations from the programmed Gaussian curvature. Finally, beyond full control over shaping, the ability to simultaneously control both $\bar{a}$ and $\bar{b}$, could open pathways for engineering exotic mechanical properties into elastic sheets.[42]

Results

Our approach comprises three stages: (1) design, in which the continuous swelling field is calculated. (2) Pixelization, in which the smooth field is digitized into the chosen resolution. (3) Fabrication, in which the desired flat structure is 3D printed (Fig. 1). The programmed geometry is actuated by hydrating the gel in water, and the material can undergo many hydration–dehydration cycles, resulting in repeatable actuation.

While this approach can be extended to fully 3D structures, here we focus on printing thin structures. Moreover, to actuate both morphing modes, two layers are necessary and sufficient. Hence, we print bilayer structures, enabling simultaneous control over both $\bar{a}$, and $\bar{b}$. The relative densities of the two voxel types dictate the local effective swelling ratio. In other words, the discrete nature of the voxelated structure, while smoothed by the elastic response of the material, yields an effective smooth reference geometry. Therefore, a critical parameter is the ratio between the sheet thickness and the voxel spatial resolution. This ratio must be sufficiently large, that is, the voxel size must be small compared to the thickness[11] (analogous to how black and white pixels produce a grayscale image when the resolution is sufficiently high. When this ratio is insufficient, the sheet can undergo local buckling at the voxel scale, causing the actuated shape to deviate from the programmed geometry. An additional design limitation is universal for shape-morphing sheets, which is the requirement that the thickness will be small. For printing cm-sized sheets, we identified a thickness of 400 μm as sufficient, and chose the voxel size to be 200 × 200 × 200 μm. Benefiting from the high resolution of our commercial DLP printers, each voxel contains approximately 30 DLP projector pixels. Moreover, the thickness of our samples is twice the voxel size and, therefore, well within the homogenization regime identified in ref. 11. This ensures that the digitization is performed at a length scale that is smoothed by elasticity, faithfully reproducing the original continuous field.

Each printed layer is formed as follows: voxels of the first material are printed, the resin bath is replaced, and then a layer of the second material is printed (Fig. 1b). For visualization purposes, we color the voxels made of the gel with the higher crosslinking density orange. The colored and uncolored voxels are referred to as ''dark'' and ''light'' voxels, respectively. This sequential printing method offers advantages over molding the second material, providing better control and flexibility while supporting the subsequent layer. The method is compatible with multi-material printers and can be generalized to an arbitrary number of materials. In the present work, this process is repeated twice to form a bilayer composite structure with the desired properties.

For each layer, the local relative spatial density of the two voxel types provides an effective swelling field. Denoting these swelling fields in the top and bottom layers, ω_t, and, ω_b, respectively, the resulting non-Euclidean reference tensors read (see SI for details):

$$\bar{a} = \frac{1}{4}(\omega_t + \omega_b)^2 \begin{pmatrix} 1 & 0 \\ 0 & 1 \end{pmatrix},\ \bar{b} = \frac{3}{t}\left(\frac{\omega_t - \omega_b}{\omega_t + \omega_b}\right)\begin{pmatrix} 1 & 0 \\ 0 & 1 \end{pmatrix} \quad (1)$$

Note that while isotropic swelling provides full control over $\bar{a}$, (*i.e.*, any reference metric can be realized), it can only prescribe isotropic curvatures. Nevertheless, it controls the sign of curvature, which is impossible when prescribing only $\bar{a}$.

Since the printed sheets are thin, they are nearly inextensible, implying that to obtain the desired configuration with metric a, ω_t and ω_b must be properly selected to yield $\bar{a} \approx a$. This also overcomes the limitation of our ability to independently control $\bar{b}$, as $\bar{a}$ induces the Gaussian curvature while $\bar{b}$ controls the mean curvature (by biasing the curvature sign). Therefore, we start by computing the metric first and then adding the curvature to each layer. In this context, it is more natural to express eqn (1) using the metric generator (average swelling), $\omega_0 \equiv \frac{1}{2}(\omega_t + \omega_b)$, and the curvature generator (swelling variation) $\kappa_0 \equiv \frac{3}{2t\omega_0}(\omega_t - \omega_b)$, which yields:

$$\bar{a} = \omega_0^2 \begin{pmatrix} 1 & 0 \\ 0 & 1 \end{pmatrix},\ \bar{b} = \kappa_0 \begin{pmatrix} 1 & 0 \\ 0 & 1 \end{pmatrix}, \quad (2)$$

where, t, is the thickness of the printed sheet.

For simple geometries, the metric generator can be analytically calculated directly from the desired shape (see SI). For more complex shapes, numerical methods, such as the Boundary First

Flattening (BFF) algorithm, can be employed to find conformal parameterizations of target surfaces.[39] Both methods involve finding a mapping from the curved surface to a plane that does not distort angles but is allowed to swell/compress different sections (Fig. 1a). We still retain the freedom of selecting κ_0 to prescribe the spontaneous curvature.

Swelling and curvature calibration

To calibrate our system, we must first determine how the swelling depends on the density of the dark voxels, ρ. To achieve this, we print square calibration structures composed of a single layer with a uniform dark-voxel density ranging from 0% to 40%. The printed structures are immersed in water until fully swollen. We verify that the swollen structures remain square and flat, confirming that the printing resolution is sufficient for the voxelated structure to yield an effective uniform swelling ratio, ω_0. When completely swollen, we measure the relative change in their length, $\omega_0 = \frac{\ell}{\ell_0}$, where ℓ and ℓ_0 are the swollen and original lengths, respectively. As expected, the lengthening is reduced as the density of the dark voxels is increased. The resulting constitutive law is nearly linear in the voxel density and exhibits a 25% relative longitudinal swelling between the extremal densities (Fig. 2a). This measurement enables calibration of the emerging reference metric, and thus to inverse design density profiles for desired shapes of plates in the thin limit.

Next, we construct sheets with uniform ω_0 (hence programming vanishing Gaussian curvature), while controlling the spontaneous curvature by prescribing gradients in the through-thickness direction (controlling κ_0). We print structures with a uniform voxel density on either the top or the bottom layer, with the other layer containing no dark voxels. Upon actuation, the swelling gradient produces a uniform curvature that can be predicted by substituting the constitutive law into eqn (2). The predicted magnitudes of the resulting curvatures match all the measurements very well, with no fitting parameters (Fig. 2b), and we demonstrate the ability to control the curvature in both directions (curving upward and downward). The uniformity of the curvature provides additional confirmation that the discrete programmed swelling field is properly homogenized.

Introducing swelling gradients

Once the constitutive law is established, we program more complicated shapes by introducing spatial gradients to the voxel densities. We begin with inducing only Gaussian morphing ($\kappa_0 = 0$). Linear radial swelling profiles, $\omega_0(r,\theta) = \alpha r + \beta$, are sufficient to induce non-vanishing Gaussian curvature. The sign of the Gaussian curvature depends on the profile's slope: increasing and decreasing trends prescribe negative and positive Gaussian (*i.e.*, saddle-like and dome-like geometries), respectively. Using this approach, we demonstrate the formation of 3D shapes governed by radial changes, such as dome-like and combined dome-saddle-like structures (Fig. 3). The dome-like regions are programmed with a positive Gaussian curvature,

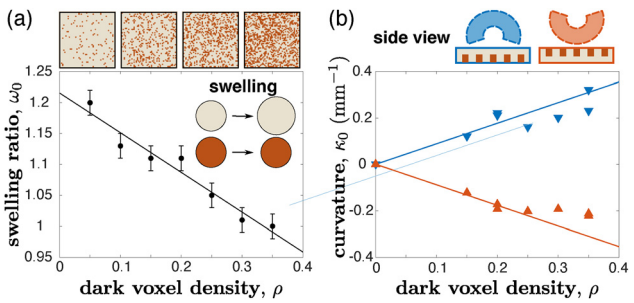

Fig. 2 Calibration measurements of swelling ratio and curvature. (a) The longitudinal swelling ratio (ratio between the actuated and original lengths), ω_0, of calibration samples with a uniform voxel density (dark circles). A fitted linear trend (black line) indicates a monotonic dependence of the swelling ratio on the voxel concentration. Relative swelling of nearly 25% was achieved, allowing significant freedom in prescribing target shapes. The variation in the voxel density is illustrated in the squares above. (b) The prescribed curvature, κ_0, for bilayer samples with one layer having uniform voxel density and the other having no dark voxels (red and blue points correspond to dark voxels only on the top or bottom layer, respectively). The solid lines result directly from substituting the swelling calibration fit from panel (a) into eqn (2) with no fitting parameters. These results demonstrate the capability to prescribe curvature in either direction and enable quantitative programming of the reference fields.

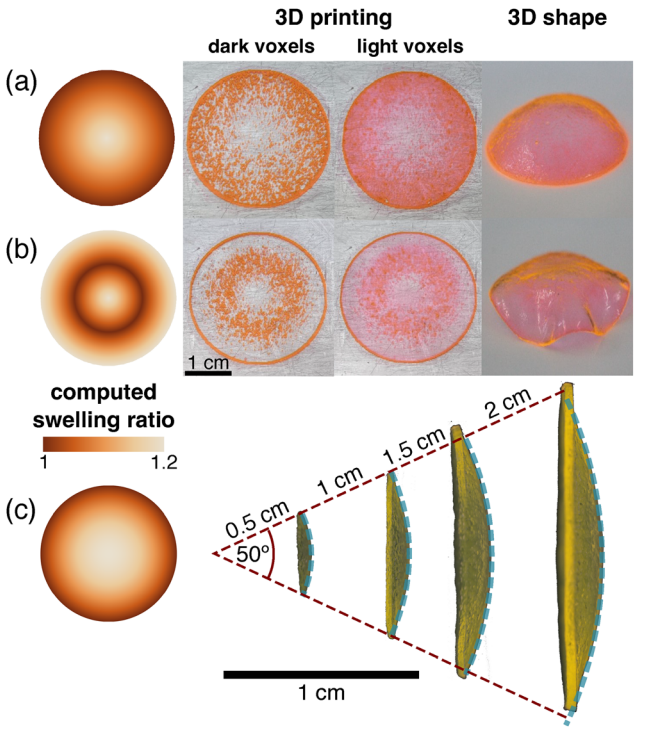

Fig. 3 Control of Gaussian morphing by inducing lateral swelling gradients. (a) and (b) Simple samples with axisymmetric swelling gradients, either increasing monotonically (a, left panel), or increasing and then decreasing (b, left panel). The programmed geometry results in a spherical structure, or a spherical center with wavy rims, due to the programmed hyperbolic geometry (right panels of a, b, respectively). (c) Printed gels with a swelling field corresponding to the metric of a sphere. We printed four samples of different sizes with reference metrics of spheres with varying radii in the range 0.5–2 cm and a fixed spherical angle of 50° (dashed teal arcs). The swollen gels adopt these configurations, as illustrated by the tight fit of the arcs.

while the saddle-like regions are programmed with a negative Gaussian curvature. The fact that the swollen structures are smooth, showing no evidence for the discretized swelling fields, provides further validation that the resolution is high enough for elastic homogenization. Our control over the shape is not merely qualitative: we calculate the swelling fields required for spherical caps with radii in the range from 0.5 to 2 cm (see SI for the calculation). Gel disks of different radii, programmed with the corresponding discretized swelling fields, are printed and actuated. The disks morph into caps with the prescribed spherical angle and radius (Fig. 3c).

Next, we test the ability to actuate the bilayer effect. To this end, we 3D print disks with uniform average voxel densities (hence, uniform ω_0), and with spatially varying programmed spontaneous curvature. Specifically, the swelling variation oscillates sinusoidally between the two layers as a function of the azimuthal angle, as shown in Fig. 4. In this case, both the spontaneous curvature sign and magnitude oscillate, bending the disk upward and downward alternately. We design and print such structures with 3, 4, 5, and 6 oscillation nodes. The resulting shapes exhibit the prescribed number of nodes, demonstrating spatial control over the direction of curvature. Note that these shapes have negligible Gaussian curvature (the curvature is predominantly uniaxial, oriented azimuthally). As such, the curvature direction is controlled while the stretching associated with these structures remains small.

The control of either the Gaussian curvature or the spontaneous curvature, as shown in Fig. 3 and 4 has been

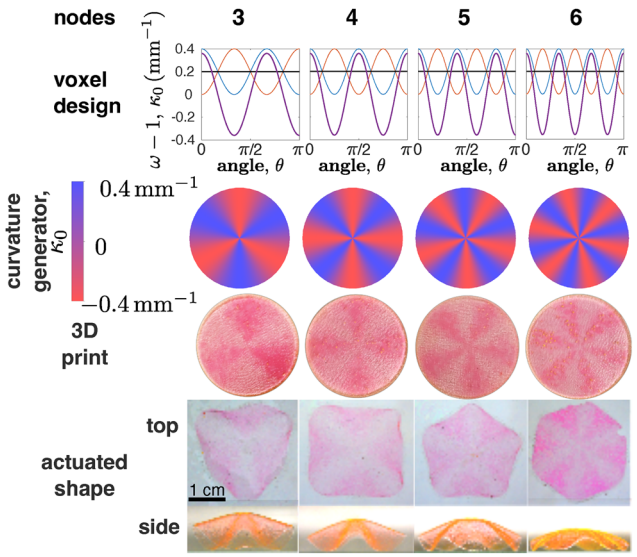

Fig. 4 Control of the bilayer effect by introducing swelling gradients across the thickness: Discs with an azimuthally oscillating spontaneous curvature and a flat reference metric. We print structures with a varying number of nodes (3, 4, 5, and 6), and printed radius: 15 mm, demonstrating our ability to induce shape by controlling the spatial distribution of the spontaneous curvature. The voxel design, plotted for only half of the disc for clarity, includes the top and bottom pixel densities (red and blue lines, respectively), and the resulting metric and curvature generators (black and purple lines, respectively). All samples are circular. The apparent polygonal contour (third row) results solely from 3D projection effects.

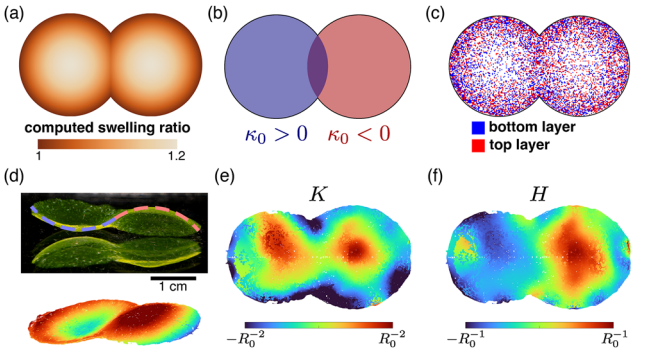

Fig. 5 A simultaneous control over Gaussian morphing and the bilayer effect. We design and print a structure composed of two identical spherical caps, each with a different spontaneous curvature direction (final radius: 15 mm, printed radius: 11 mm, overlap: 4.4 mm). (a) The reference metric is the same for both halves and is identical to that in Fig. 3. (b) The spontaneous curvature is uniform in each half, equal in magnitude to the curvature encoded in the reference metric, but with opposite signs. (c) The resulting voxel map, where color indicates the layer of each dark voxel (blue – top layer, red – bottom layer). (d) The swollen sample (and its reflection) demonstrates simultaneous control over both reference fields (top). The dashed line corresponds to the programmed radius of curvature, illustrating quantitative agreement with the designed configuration. The sample is 3D scanned and smoothed (bottom). (e, f) The calculated Gaussian and mean curvatures illustrate the double-dome structure.

demonstrated in earlier works.[8,11,13] However, the simultaneous control over both quantities, which is essential for complete control over the shape, has not yet been achieved. We now utilize our ability to independently control both morphing modes to achieve this goal, that is, inducing both Gaussian morphing and the bilayer effect, simultaneously. To this end, we design a model that requires both Gaussian curvature and spatial control over the curvature sign: two spherical caps with a small overlap (Fig. 5) curved in opposite directions. Each cap has the same swelling ratio of a spherical cap used in Fig. 3c (*i.e.*, the same ω_0 field), but an opposite sign of the spontaneous curvature (*i.e.*, opposite κ_0 fields). The magnitude of the spontaneous curvature is designed to match the radius of curvature of the sphere, and its sign changes from positive in the left half to negative in the right half (κ_0 vanishes in the overlap region). These two conditions determine ω_0 and κ_0, and hence, the complete design. All printed structures robustly morphed into the designed double-dome shape, with a positive and negative mean curvature in the respective domes. The radius of curvature of each half matches the programmed value quantitatively (Fig. 5d). These results highlight the advantage of our method, as achieving this configuration is impossible when controlling only one of the two reference fields.

Discussion and conclusions

This work presents a novel strategy based on 3D printing to design and fabricate self-morphing sheets of smart materials with programmable responsive geometry. Until now, experimental realizations of self-morphing have been limited to actuating either the bilayer effect or Gaussian morphing, thereby

providing only partial control over the final configuration. A recent machine-learning approach[40] addresses the inverse design of non-Euclidean plates using only Gaussian morphing. In contrast, our mechanics-based framework independently controls both morphing modes, enabling structures such as those in Fig. 4 and 5 that are inaccessible by that approach. Here, we advance beyond the state of the art by developing a method that fully programs the swelling field, actuating both modes simultaneously. In our approach, the 3D printer is not used to explicitly build a 3D structure. Instead, we utilize its high resolution and accuracy to encode digital information into a thin, flat sample. Upon actuation, this information drives the self-morphing of the sheet into the desired, accurately predicted, 3D shape. This strategy of using a printer as a programming machine, implementing digitization, and separating lateral and through-thickness gradients, applies broadly to other responsive materials, suggesting a new general paradigm for self-morphing. In this work, we limited the study to isotropic swelling, which provides control over the direction of curvature. We hypothesize that other homogenization schemes may provide even further control over the reference geometry. While our approach allows printing structures with an arbitrary number of layers, we limited the study to bilayer structures as those are sufficient to fully program Gaussian morphing and the bilayer effect. Our approach allows printing additional layers. Moreover, there is a strong interest in a shape-morphing structure that can operate under orthogonal actuation modes (such as temperature and pH), which is not straightforward using traditional fabrication techniques.[43] However, with our system, achieving this simply requires printing voxels composed of various responsive materials with the necessary actuation modes, similar to how grayscale printing is extended to color printing by adding pixels of different colors.

Combining computational design of the swelling field needed for obtaining a desired 3D shape with pixelization makes our approach compatible with all common 3D printers based on stereolithography processes, enabling fabrication using only two materials, thus simplifying the fabrication process. The ability to control both the metric and the curvature opens new directions for 4D design. 3D structures can be made fully compatible (*i.e.*, having a compatible reference metric and curvature) and thus possess a single, well-defined equilibrium shape, as in Fig. 5. Alternatively, structures can be designed to be weakly or strongly incompatible. As the degree of incompatibility increases, the resulting structures possess many metastable configurations, making them more responsive mechanically. We note that, beyond enabling specification of a desired 3D shape, the ability to accurately control both metric and curvature can be utilized to fabricate structures with exotic mechanical properties,[42] significantly expanding the concept of ''smart materials''. Another advantage of our strategy is that it is material-agnostic, hence can be easily extended to other responsive materials. Here, we use hydrogels that swell uniformly with different magnitudes. Other uniformly swelling candidates are inter-diffusing polymers. Moreover, in many cases, introducing gradients by controlling the swelling orientation (such as in nematic elastomers, for instance) is advantageous.[10,28,44] While the design stage for these materials is different,[45] the pixelization can follow the same algorithm. Therefore, we provide a pathway to employ 4D printing across diverse responsive materials, unlocking diverse applications from soft robotics and deployable aerospace structures to biomedical scaffolds and drug delivery devices, while enabling programmable mechanical properties and multi-stimuli responsive systems that can operate under orthogonal actuation modes such as temperature, pH, humidity, or light.

Materials and methods

Acrylic acid was purchased from Acros (Belgium). TPO photoinitiator diphenyl(2,4,6-trimethylbenzoyl)phosphine oxide was obtained from BASF (Germany). The surfactant SDS, sodium dodecyl sulfate, and dye rhodamine 6G were purchased from Sigma Aldrich (Merck, Germany). PEGDA was obtained as a gift from Sartomer-Arkema (France). Triple distilled water (TDW) was obtained from NANOpure®-DIamondTM (TDW; 0.0055 μS cm^{-1}; Barnsted system, IA, USA).

Digitization of the concentration fields

Once the desired $\bar{a}$ and $\bar{b}$ are calculated, we extract the metric and curvature generators, ω_0, and Δ, and then calculate the smooth density field of each layer. Then, each voxel is assigned a material independently according to the local density value. For instance, if the local density value is 0.2, the probability that it will be assigned a dark or a light voxel, is 20% and 80%, respectively.

Printing formulation

The printing compositions are based on materials previously developed in our lab.[22] Two types of UV-curable aqueous solutions inks, containing acrylic acid with polyethylene glycol diacrylate (PEGDA) as a crosslinker were prepared: one with low wt% of PEGDA (2 wt% PEGDA, 38 wt% acrylic acid, TDW 58 wt%) and another with high wt% of PEGDA (6 wt% PEGDA, 34 wt% acrylic acid, TDW 58 wt%). For both printing compositions, 2 wt% of the photoinitiator, Diphenyl(2,4,6-trimethylbenzoyl)phosphine oxide (TPO) in the form of water dispersible nanoparticles were added (with ionic SDS as a surfactant). All the materials were stirred together until the photoinitiator powder was fully dispersed and a clear solution was obtained. Rhodamine 6G was added as a dye to the solution with a high wt% of PEGDA, to distinguish between the solutions.

Multi-material 3D printing

The inks were printed with a DLP printer (Pico2, Asiga, Australia) with a 385nm UV-LED light source. Each printed layer's thickness was 200 μm, with a light intensity of 25 mW cm^{-2} and exposure times of 3 and 4 seconds, for the high and low PEGDA wt%, respectively. The dual-material printing was utilized by pausing the printing and switching the baths. In total,

three bath replacements were conducted to form two multi-material layers.

Author contributions

I. L., E. Sh, and S. M. designed the research. I. L. designed the printed structures. E. Sa., R. L., and N. B. printed the hydrogel sheets. I. L. measured the induced shape transformations. I. L., E. Sa, E. Sh, and S. M. wrote the manuscript and produced the figures. E. Sh. and S. M. have jointly supervised the work.

Conflicts of interest

There are no conflicts to declare.

Data availability

The data supporting this article have been deposited in Borealis. See DOI: https://doi.org/10.5683/SP3/LVQED8. Supplementary calculations are included as part of the supplementary information (SI). See DOI: https://doi.org/10.1039/d5sm00780a.

Acknowledgements

This research is supported by the National Research Foundation, Prime Minister's Office, Singapore, under its Campus of Research Excellence and Technological Enterprise (CREATE) Program, by the United States–Israel Binational Science Foundation (grant 2020739), and by the Israel Science Foundation (grants 2437/20). I.L. was supported by the Washington Research Foundation, the Azrieli Foundation, and the Fulbright Foundation.

Notes and references

1 M. Yoneda, Y. Kobayakawa, H. Y. Kubota and M. Sakai, *J. Cell Sci.*, 1982, **54**, 35–46.
2 U. Nath, B. C. W. Crawford, R. Carpenter and E. Coen, *Science*, 2003, **299**, 1404–1407.
3 S. Armon, M. S. Bull, A. Aranda-Diaz and M. Prakash, *Proc. Natl. Acad. Sci. U. S. A.*, 2018, **115**, E10333–E10341.
4 S. Armon, E. Efrati, R. Kupferman and E. Sharon, *Science*, 2011, **333**, 1726–1730.
5 S. Guest, E. Kebadze and S. Pellegrino, *J. Mech. Mater. Struct.*, 2011, **6**, 203–212.
6 M. Pezzulla, G. P. Smith, P. Nardinocchi and D. P. Holmes, *Soft Matter*, 2016, **12**, 4435–4442.
7 E. Siéfert, I. Levin and E. Sharon, *Phys. Rev. X*, 2021, **11**, 011062.
8 Y. Klein, E. Efrati and E. Sharon, *Science*, 2007, **315**, 1116–1120.
9 M. E. McConney, A. Martinez, V. P. Tondiglia, K. M. Lee, D. Langley, I. I. Smalyukh and T. J. White, *Adv. Mater.*, 2013, **25**, 5880–5885.
10 H. Aharoni, Y. Xia, X. Zhang, R. D. Kamien and S. Yang, *Proc. Natl. Acad. Sci. U. S. A.*, 2018, **115**, 7206–7211.
11 J. Kim, J. A. Hanna, M. Byun, C. D. Santangelo and R. C. Hayward, *Science*, 2012, **335**, 1201–1205.
12 Z. L. Wu, M. Moshe, J. Greener, H. Therien-Aubin, Z. Nie, E. Sharon and E. Kumacheva, *Nat. Commun.*, 2013, **4**, 1586.
13 A. Nojoomi, J. Jeon and K. Yum, *Nat. Commun.*, 2021, **12**, 603.
14 E. Hajiesmaili and D. R. Clarke, *Nat. Commun.*, 2019, **10**, 183.
15 H. G. Schild, *Prog. Polym. Sci.*, 1992, **17**, 163–249.
16 Y. Dong, S. Wang, Y. Ke, L. Ding, X. Zeng, S. Magdassi and Y. Long, *Adv. Mater. Technol.*, 2020, **5**, 2000034.
17 Y. Hirokawa and T. Tanaka, *J. Chem. Phys.*, 1984, **81**, 6379–6380.
18 H. Banerjee, M. Suhail and H. Ren, *Biomimetics*, 2018, **3**, 15.
19 D. Han, C. Farino, C. Yang, T. Scott, D. Browe, W. Choi, J. W. Freeman and H. Lee, *ACS Appl. Mater. Interfaces*, 2018, **10**, 17512–17518.
20 L. Larush, I. Kaner, A. Fluksman, A. Tamsut, A. A. Pawar, P. Lesnovski, O. Benny and S. Magdassi, *J. 3D Print. Med.*, 2017, **1**, 219–229.
21 A. A. Pawar, S. Halivni, N. Waiskopf, Y. Ben-Shahar, M. Soreni-Harari, S. Bergbreiter, U. Banin and S. Magdassi, *Nano Lett.*, 2017, **17**, 4497–4501.
22 A. A. Pawar, G. Saada, I. Cooperstein, L. Larush, J. A. Jackman, S. R. Tabaei, N.-J. Cho and S. Magdassi, *Sci. Adv.*, 2016, e1501381.
23 Q. Ge, Z. Chen, J. Cheng, B. Zhang, Y.-F. Zhang, H. Li, X. He, C. Yuan, J. Liu, S. Magdassi and S. Qu, *Sci. Adv.*, 2021, eaba4261.
24 M. Hua, D. Wu, S. Wu, Y. Ma, Y. Alsaid and X. He, *ACS Appl. Mater. Interfaces*, 2021, **13**, 12689–12697.
25 C. B. Highley, C. B. Rodell and J. A. Burdick, *Adv. Mater.*, 2015, **27**, 5075–5079.
26 S. Liu and L. Li, *ACS Appl. Mater. Interfaces*, 2017, **9**, 26429–26437.
27 L. Huang, R. Jiang, J. Wu, J. Song, H. Bai, B. Li, Q. Zhao and T. Xie, *Adv. Mater.*, 2017, **29**, 1605390.
28 A. Sydney Gladman, E. A. Matsumoto, R. G. Nuzzo, L. Mahadevan and J. A. Lewis, *Nat. Mater.*, 2016, **15**, 413–418.
29 Y. Zhou, C. M. Duque, C. D. Santangelo and R. C. Hayward, *Adv. Funct. Mater.*, 2019, **29**, 1905273.
30 J. W. Boley, W. M. van Rees, C. Lissandrello, M. N. Horenstein, R. L. Truby, A. Kotikian, J. A. Lewis and L. Mahadevan, *Proc. Natl. Acad. Sci. U. S. A.*, 2019, **116**, 20856–20862.
31 E. Efrati, E. Sharon and R. Kupferman, *J. Mech. Phys. Solids*, 2009, **57**, 762–775.
32 Y. Klein, S. Venkataramani and E. Sharon, *Phys. Rev. Lett.*, 2011, **106**, 118303.
33 C. Huang, Z. Wang, D. Quinn, S. Suresh and K. J. Hsia, *Proc. Natl. Acad. Sci. U. S. A.*, 2018, **115**, 12359–12364.
34 E. Sharon, B. Roman and H. L. Swinney, *Phys. Rev. E*, 2007, **75**, 046211.

35 T. Portet, Z. R. Cohen, G. J. Goetz, N. Panek, P. N. Holmes, S. A. Stephens, T. Varga and S. L. Keller, *Biophys. J.*, 2022, **121**, 2389–2397.
36 I. Levin and E. Sharon, *Phys. Rev. Lett.*, 2016, **116**, 035502.
37 D. Grossman, E. Sharon and H. Diamant, *Phys. Rev. Lett.*, 2016, **116**, 258105.
38 K. Sun and X. Mao, *Phys. Rev. Lett.*, 2021, **127**, 98001.
39 R. Sawhney and K. Crane, *ACM Trans. Graph.*, 2018, **37**, 1–14.
40 X. Sun, L. Yue, L. Yu, C. T. Forte, C. D. Armstrong, K. Zhou, F. Demoly, R. R. Zhao and H. J. Qi, *Nat. Commun.*, 2024, **15**, 5509.
41 J. Panetta, F. Isvoranu, T. Chen, E. Siéfert, B. Roman and M. Pauly, *ACM Trans. Graph.*, 2021, **40**, 1–14.
42 M. Arieli, M. Moshe and E. Sharon, *Soft Matter*, 2024, **20**, 4414–4421.
43 H. Thérien-Aubin, Z. L. Wu, Z. Nie and E. Kumacheva, *J. Am. Chem. Soc.*, 2013, **135**, 4834–4839.
44 J. Gu, D. E. Breen, J. Hu, L. Zhu, Y. Tao, T. Van De Zande, G. Wang, Y. J. Zhang and L. Yao, Conference on Human Factors in Computing Systems - Proceedings, 2019, 1–10.
45 I. Griniasty, H. Aharoni and E. Efrati, *Phys. Rev. Lett.*, 2019, **123**, 127801.